Measurement of in-plane and out-of-plane displacements and strains using digital holographic moiré

Rishikesh Kulkarni[a], Sai Siva Gorthi[b] & Pramod Rastogi[a]

[a] Applied Computing and Mechanics Laboratory, Ecole Polytechnique Federale de Lausanne, Lausanne, Switzerland.

[b] Department of Instrumentation and Applied Physics, Indian Institute of Science, Bangalore, India.
Published online: 28 Apr 2014.

PLEASE SCROLL DOWN FOR ARTICLE

Taylor & Francis
Taylor & Francis Group

Measurement of in-plane and out-of-plane displacements and strains using digital holographic moiré

Rishikesh Kulkarni[a], Sai Siva Gorthi[b] and Pramod Rastogi[a*]

[a]*Applied Computing and Mechanics Laboratory, Ecole Polytechnique Federale de Lausanne, Lausanne, Switzerland;* [b]*Department of Instrumentation and Applied Physics, Indian Institute of Science, Bangalore, India*

The paper proposes a non-destructive method for simultaneous measurement of in-plane and out-of-plane displacements and strains undergone by a deformed specimen from a single moiré fringe pattern obtained on the specimen in a dual beam digital holographic interferometry setup. The moiré fringe pattern encodes multiple interference phases which carry the information on multidimensional deformation. The interference field is segmented in each column and is modeled as multicomponent quadratic/cubic frequency-modulated signal in each segment. Subsequently, the product form of modified cubic phase function is used for accurate estimation of phase parameters. The estimated phase parameters are further utilized for direct estimation of the unwrapped interference phases and phase derivatives. The simulation and experimental results are provided to validate the effectiveness of the proposed method.

Keywords: digital holographic moiré; interferometry; multicomponent signal; in-plane and out-of-plane displacements and strains; modified cubic phase function

1. Introduction

Over the years, several fringe analysis techniques have been proposed to accurately estimate the interference phase and which have significantly impacted deformation measurement systems in the broad field of optical metrology. Some of these techniques are based on the Fourier transform [1], the windowed Fourier transform [2], the wavelet transform [3], the regularized phase tracking [4], the piecewise polynomial phase approximation [5,6], etc. However, the fringe analysis techniques mentioned above have been developed with a view to be plugged onto the measurement systems dedicated to single deformation measurements which produce fringe patterns having a single-interference phase map. These single-phase measurement systems are, in general, dedicated to the measurement of quantities such as contouring [7], or single displacement components [8,9]. However, a major drawback of the fringe analysis techniques cited above [1–6] is that they fail when applied to the simultaneous measurement of multiple displacement components. Hence, there is an important need for the development of fringe analysis techniques for multidimensional deformation measurement. The scope of our paper will be focused on the development of such measurement systems in the context of digital holography. The scale of importance of digital holography in optical metrology has significantly increased by its ability to use a charge-coupled device (CCD) to record the interference of an object beam and a reference beam.

The problem of multidimensional deformation measurement has led to the investigation of new techniques based on the use of multiple object-reference beam pairs in digital holographic interferometry. In Ref. [10], a multiplexing-demultiplexing technique for digitally recorded holograms is developed that basically involves obtaining an incoherent mixing of two object waves scattered from an object surface. To each of the scattered wave is assigned a separate reference beam. Each of the two pairs of object-reference beams are orthogonally polarized one with respect to the other. On the other hand, the work in Ref. [11] is based on the use of delay lines to obtain multiple sets of independent holograms on one single CCD frame. Although requiring complicated setups, these methods have been successfully applied to the simultaneous measurement of multiple displacement components of an object subjected to load. Other elegant methods have been reported in Refs. [12,13], which have maintained the basic precept of incoherent mixing of scattered object waves using multiple pairs of object and reference beams, with each pair originating from a laser of a different wavelength. The price to pay here is the use of multiple lasers in a measurement system. Finally, Ref. [14] considers sequentially recording a pair of digital holograms for each of the two object-reference beam pairs

---

used in the measurement system. However, the requirement of multiple frames and the use of sequential recording makes the method less relevant to the simultaneous measurement of multiple displacement components of a dynamic object.

We have recently developed a digital holographic moiré-based system [15] that overcomes the need to optically obtain multiple pairs of object-reference beams, by simultaneously illuminating the object from multiple directions and using a single reference beam. The method has been shown to be effective in the simultaneous measurement of in-plane and out-of-plane components of displacements of a deformed object. However, the method in Ref. [15] requires a careful control of the carrier in the experimental setup to ensure the separation of the signal components in the frequency domain. Although the techniques proposed in [16,17] overcome this problem, these techniques are applied only for the multidimensional displacement measurement. Moreover, whereas the phase estimation method proposed in [16] is sensitive to noise, the interference phase approximation method in [17] is limited upto second-order polynomial.

In the present paper, we propose a new method for simultaneous estimation of multiple interference phases and their derivatives from a single digital holographic moiré fringe pattern. A multicomponent local quadratic/cubic frequency-modulated signal model of the interference field is considered which allows to approximate the rapidly varying interference phases with lower order polynomial phase function. Consequently, the method provides the flexibility to select either the third-order or the fourth-order polynomial phase approximation. The proposed method relies on the product form of modified cubic phase function (MCPF) for accurate estimation of the polynomial coefficients. The estimated polynomial coefficients are utilized for estimating the multiple unwrapped interference phases and phase derivatives. The theory of proposed method is explained in the next section. Simulation and experimental results are provided in Section 3, followed by conclusions.

2. Theory

Consider two-directional illumination of an object surface with two illumination beams oriented symmetrically with respect to the surface normal. The holograms are recorded before and after deformation of the object. The conjugate multiplication of reconstructed optical wavefields corresponding to the different object states results in a multi-component interference field which can be represented as,

$$\gamma(x, y) = A_1(x, y) \exp[j\phi_1(x, y)]$$
$$+ A_2(x, y) \exp[j\phi_2(x, y)] + \eta(x, y) \quad (1)$$

We note that the interference field $\gamma(x, y)$ of size $N \times N$ contains two signal components. $A_1(x, y)$ and $A_2(x, y)$ are assumed to be slowly varying or of constant amplitudes; $\phi_1(x, y)$ and $\phi_2(x, y)$ are the interference phases

corresponding to the two object beams; and, $\eta(x, y)$ is the complex additive white Gaussian noise. In the proposed optical configuration, the sum and difference of interference phases provides the measurement of out-of-plane and in-plane displacement components, respectively. Similarly, the sum and difference of interference phase derivatives provides the measurement of out-of-plane and in-plane strain components, respectively. In a given column x, the interference field can be given as,

$$\gamma(y) = A_1(y) \exp[j\phi_1(y)] + A_2(y) \exp[j\phi_2(y)] + \eta(y) \quad (2)$$

In the proposed method, in each column x, $\gamma(y)$ is divided into N_w non-overlapping segments. The interference field in each segment is then approximated as a multicomponent quadratic/cubic frequency-modulated signal. The analysis is carried out for multicomponent quadratic frequency-modulated signal model. The signal length N_s in each segment is assumed to be an odd number. Further, in the segment i of the given column x where $i \in [1, N_w]$, the interference field can be represented as,

$$\gamma_i(y) = A_{1i}(y) \exp[j\phi_{1i}(y)] + A_{2i}(y) \exp[j\phi_{2i}(y)] + \eta_i(y) \quad (3)$$

where, $-\frac{(N_s-1)}{2} \leq y \leq \frac{(N_s-1)}{2}$. The interference phases can be represented as,

$$\phi_{1i}(y) = a_{i0} + a_{i1}y + a_{i2}y^2 + a_{i3}y^3 \quad (4)$$
$$\phi_{2i}(y) = b_{i0} + b_{i1}y + b_{i2}y^2 + b_{i3}y^3 \quad (5)$$

The phase derivatives along y-axis can be calculated as follows,

$$\frac{\partial \phi_{1i}(y)}{\partial y} = a_{i1} + 2a_{i2}y + 3a_{i3}y^2 \quad (6)$$

$$\frac{\partial \phi_{2i}(y)}{\partial y} = b_{i1} + 2b_{i2}y + 3b_{i3}y^2 \quad (7)$$

From Equations (4)–(7), it is evident that the phases and their derivatives' estimates can be obtained by accurately estimating the polynomial coefficients. We propose to use the product form of MCPF to calculate the estimates of a_{i3} and b_{i3}. The product form of MCPF can be written as [18],

$$\text{PMCPF}(\Omega; y_K) = \prod_{k=1}^{K} \text{MCPF}\left(y_k, \frac{y_K}{y_k}\Omega\right) \quad (8)$$

where,

$$\text{MCPF}(y, \Omega) = \sum_{m=0}^{\frac{(N_s-1)}{2}} \gamma_i(y+m)\gamma_i(y-m)$$
$$\times \gamma_i^*(-y+m)\gamma_i^*(-y-m) \exp(-j\Omega m^2) \quad (9)$$

One of the important advantages of using the product form of the MCPF function is that it allows for avoiding the effect of cross-terms and spurious peaks appearing in the case of multicomponent signal analysis. Here, K is the number of y values for which MCPF is calculated. The

spectral scaling operation in Equation (8) ensures that the peaks are aligned at single frequency calculated for each value of y. To ease the implementation, the values of y are selected as $y_K = 2y_{K-1} = 4y_{K-2} = \cdots = 2^{K-1}y_1$. Two peaks are observed in PMCPF spectrum corresponding to a_{i3} and b_{i3}. However, the difference between the two peaks is not observable. This increases the complexity of assigning coefficients to their respective polynomials. We approach this problem by modeling an amplitude discrimination criteria. The basis of this discrimination criteria is to create a sufficiently large difference between the amplitudes A_1 and A_2. The application of this criteria means that in a given optical setup, one laser beam will be set to have more intensity than the other beam. This insures that in case of $A_1 > A_2$, only a single peak corresponding to a_{i3} is observed in the PMCPF spectrum. Consequently, the estimate of coefficient a_{i3} can be obtained as,

$$\hat{a}_{i3} = \frac{\arg\max_\Omega |\text{PMCPF}(\Omega; y_K)|}{12 y_K} \tag{10}$$

Once the estimate of a_{i3} has been obtained, peeling off operation is performed as follows,

$$\gamma_{i2}(y) = \gamma_i(y) \exp\left(-j\hat{a}_{i3} y^3\right) \tag{11}$$

As a result, the signal $\gamma_{i2}(y)$ contains the second-order polynomial phase of the stronger component. Subsequently, the product cubic phase function (PCPF) is applied to obtain the estimate of a_{i2} [19]. The PCPF is computed as a product of cubic phase function (CPF) calculated for different values of y,

$$\text{PCPF}(\Omega) = \prod_{k=1}^{K} \text{CPF}(y_k, \Omega) \tag{12}$$

where,

$$\text{CPF}(y, \Omega) = \sum_{m=0}^{\frac{(N_s-1)}{2}} \gamma_{i2}(y+m)\gamma_{i2}(y-m) \exp(-j\Omega m^2) \tag{13}$$

Here, K is the number of y values for which PCPF is calculated. The dominant peak in the PCPF spectrum gives the estimate of a_{i2} as,

$$\hat{a}_{i2} = \frac{\arg\max_\Omega |\text{PCPF}(\Omega)|}{2} \tag{14}$$

To obtain the first-order coefficient estimate of the stronger component, peeling off operation is performed as follows,

$$\gamma_{i1}(y) = \gamma_{i2}(y) \exp\left(-j\hat{a}_{i2} y^2\right) \tag{15}$$

Consequently, $\gamma_{i1}(y)$ contains first-order phase of the stronger component. The estimate of a_{i1} is obtained by computing the discrete Fourier transform (DFT) of the signal $\gamma_{i1}(y)$ where,

$$X_{i1}(\omega) = \text{DFT}[\gamma_{i1}(y)] \tag{16}$$

$$\hat{a}_{i1} = \arg\max_\omega |X_{i1}(\omega)| \tag{17}$$

The DFT of $\gamma_{i1}(y)$ is computed using the Fast Fourier Transform (FFT) algorithm. The dominant peak of FFT spectrum gives coarse estimate of a_{i1}. Subsequently, a fine estimate $\hat{a}_{i1}$ is obtained using iterative frequency estimation by interpolation on Fourier coefficients [20]. Finally, $\gamma_{i1}(y)$ is peeled off to obtain the estimates for a_{i0} and A_{i1} as,

$$\gamma_{i0}(y) = \gamma_{i1}(y) \exp(-j\hat{a}_{i1} y) \tag{18}$$

$$\hat{a}_{i0} = angle\left[\frac{1}{N_s} \sum_{y=-\frac{(N_s-1)}{2}}^{\frac{(N_s-1)}{2}} \gamma_{i0}(y)\right] \tag{19}$$

$$\hat{A}_{1i} = \left|\frac{1}{N_s} \sum_{y=-\frac{(N_s-1)}{2}}^{\frac{(N_s-1)}{2}} \gamma_{i0}(y)\right| \tag{20}$$

The approximation of stronger component $\gamma_{A_{1i}}(y)$ is obtained using the coefficient estimates $\left[\hat{a}_{i3}, \hat{a}_{i2}, \hat{a}_{i1}, \hat{a}_{i0}\right]$ and the amplitude estimate $\hat{A}_{1i}$ as,

$$\gamma_{A_{1i}}(y) = \hat{A}_{1i} \exp\left[j\left(\hat{a}_{i0} + \hat{a}_{i1}y + \hat{a}_{i2}y^2 + \hat{a}_{i3}y^3\right)\right] \tag{21}$$

The contribution of stronger signal component is removed from original signal by subtracting $\gamma_{A_{1i}}(y)$ from $\gamma_i(y)$. Thus, we obtain,

$$\gamma_{A_{2i}}(y) = \gamma_i(y) - \gamma_{A_{1i}}(y) \tag{22}$$

Consequently, the effective signal primarily contains the signal component having a lower amplitude A_{2i}. The above procedure of coefficient and amplitude estimation is repeated to obtain $\left[\hat{b}_{i3}, \hat{b}_{i2}, \hat{b}_{i1}, \hat{b}_{i0}\right]$ and $\hat{A}_{2i}$ related to $\gamma_{A_{2i}}(y)$. Further, a multicomponent coefficient optimization routine [21], which involves Nelder-Mead simplex algorithm, is used for the refinement of the coefficient estimates. This procedure helps in minimizing the effect of noise and the cross-component contribution. These refined coefficient estimates along with Equations (4)–(7) are used to obtain the estimates of phases and their derivatives. It should be noted that the phases and their derivatives calculated on a segment are unwrapped. The phases $\phi_{1i}(y)$, $\phi_{2i}(y)$ and their derivatives $\frac{\partial \phi_{1i}(y)}{\partial y}$, $\frac{\partial \phi_{2i}(y)}{\partial y}$ are estimated for all the segments in all columns. Phase-stitching operation is applied to obtain 2D continuous phase distribution.

If the cubic frequency modulated signal model is considered in the event of a relatively rapidly varying interference phases, then the Equations (4)–(7) will contain additional terms with the fourth-order polynomial coefficients a_{i4} and b_{i4}. After peeling off operation in Equation (11), the coefficient a_{i4} can be calculated in similar manner as a_{i3} with the modifications in Equations (8)–(9) as,

$$\text{PMCPF}(\Omega; y_K) = \prod_{k=1}^{K} \text{MCPF}\left(y_k, \left(\frac{y_K}{y_k}\right)^2 \Omega\right) \tag{23}$$
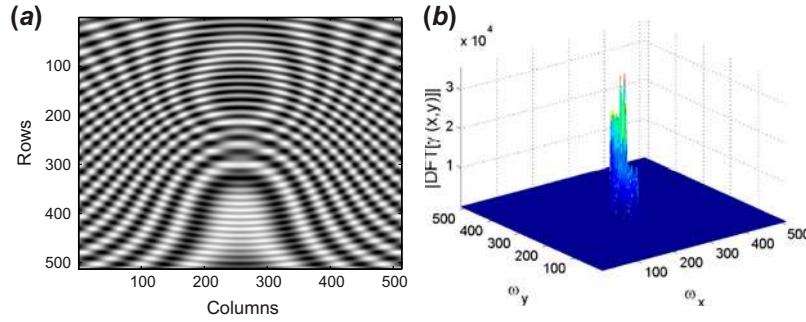
Figure 1. (*a*) Moiré fringe pattern (*b*) Fourier spectrum. (The color version of this figure is included in the online version of the journal.)
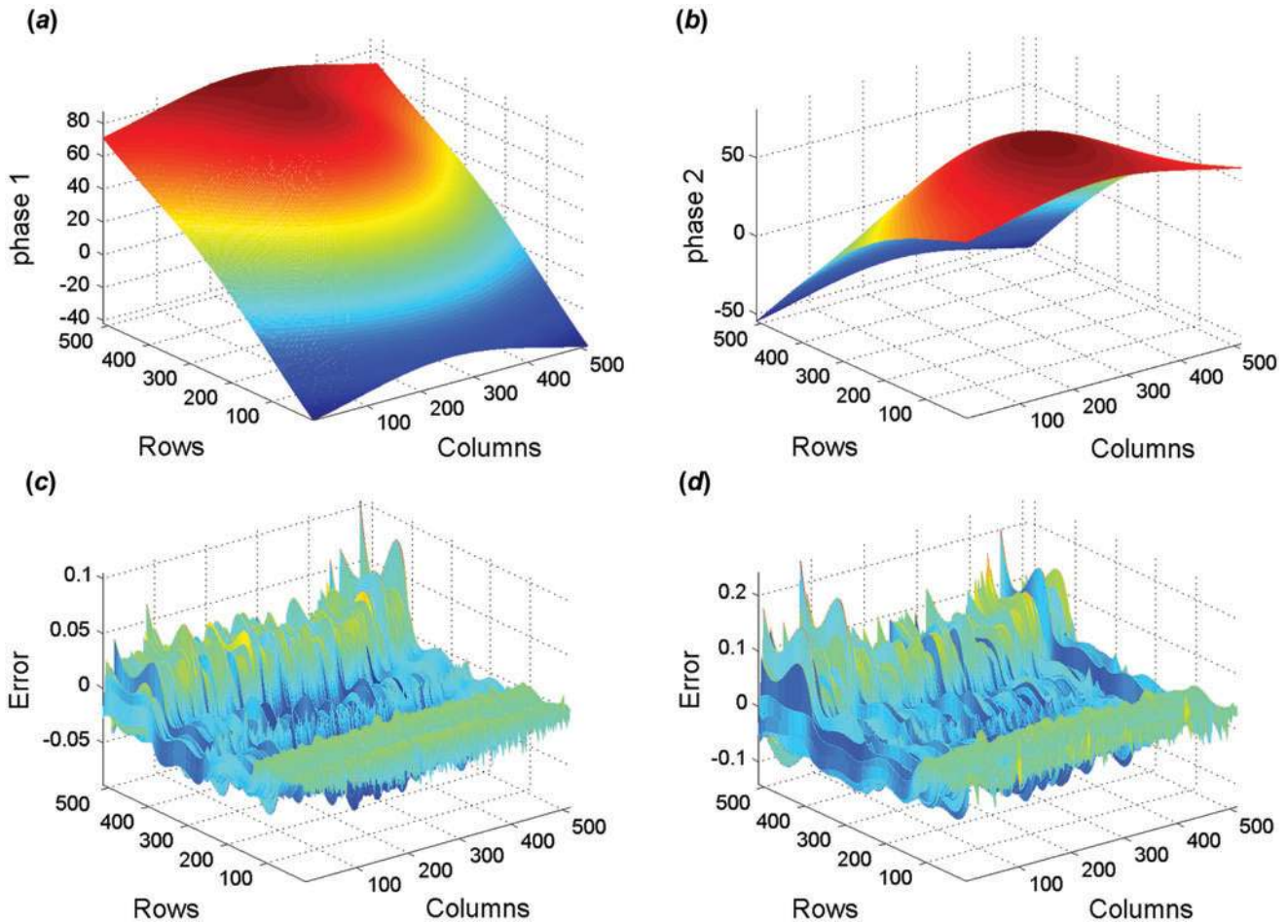

Figure 2. (*a*) Phase ϕ_1, (*b*) Phase ϕ_2, (*c*) Error in estimation of ϕ_1 and (*d*) Error in estimation of ϕ_2. All values are in radians. (The color version of this figure is included in the online version of the journal.)

where,

$$\mathrm{MCPF}(y, \Omega) = \sum_{m=0}^{\frac{(N_s-1)}{2}} \gamma_{i2}(y + m)\gamma_{i2}(y - m)$$
$$\times \gamma_{i2}^*(m)\gamma_{i2}^*(-m) \exp\left(-j\Omega m^2\right) \quad (24)$$

The estimate of coefficient a_{i4} can be calculated as,

$$\hat{a}_{i4} = \frac{\arg\max_\Omega |\mathrm{PMCPF}(\Omega; y_K)|}{12y_K^2} \quad (25)$$

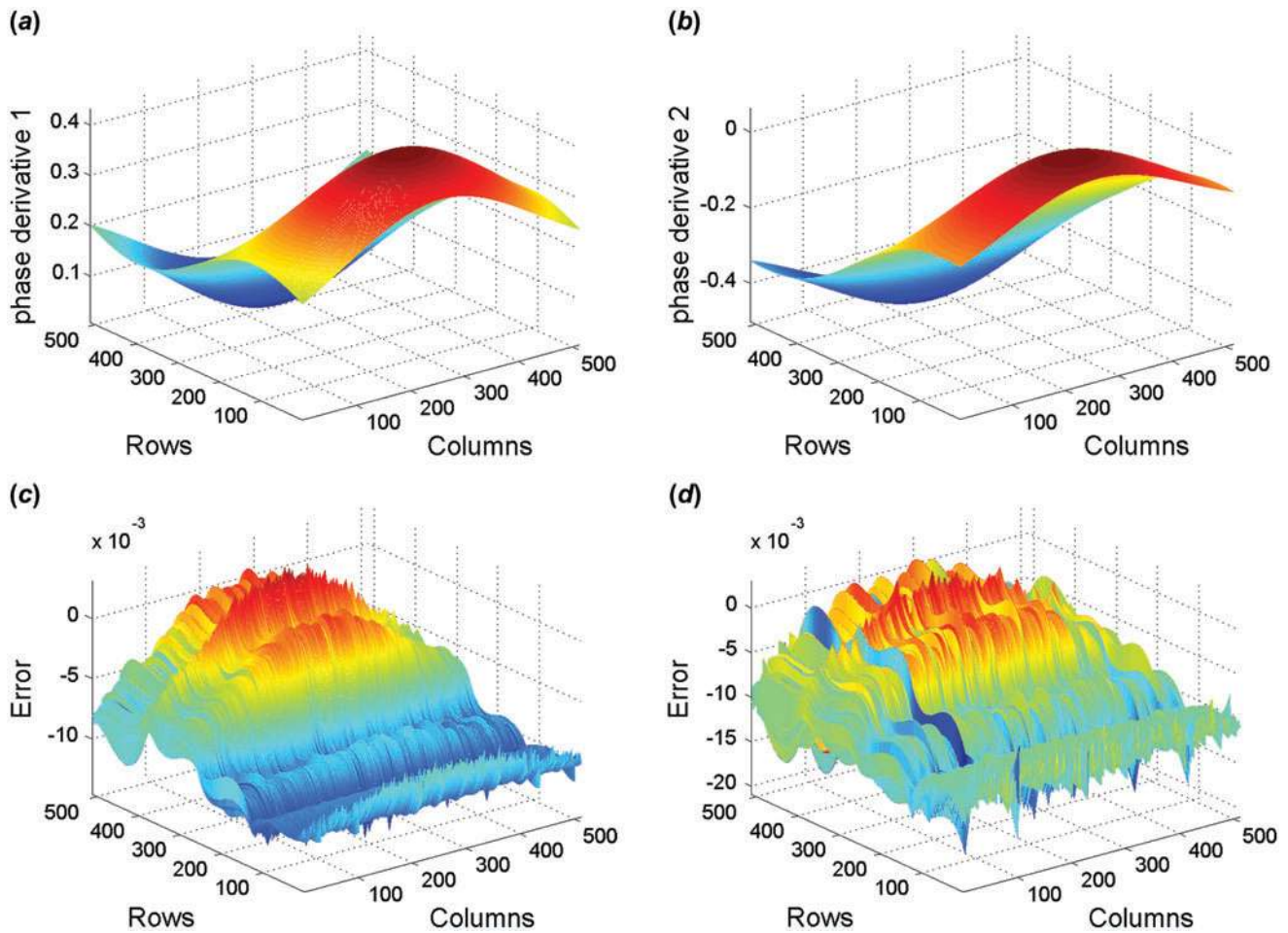Subsequently, the peeling off operation is performed to obtain the lower order polynomial coefficients.

Figure 3. (*a*) Phase derivative $\frac{\partial \phi_1(y)}{\partial y}$, (*b*) Phase derivative $\frac{\partial \phi_2(y)}{\partial y}$, (*c*) Error in estimation of $\frac{\partial \phi_1(y)}{\partial y}$ and (*d*) Error in estimation of $\frac{\partial \phi_2(y)}{\partial y}$. All values are in radians. (The color version of this figure is included in the online version of the journal.)
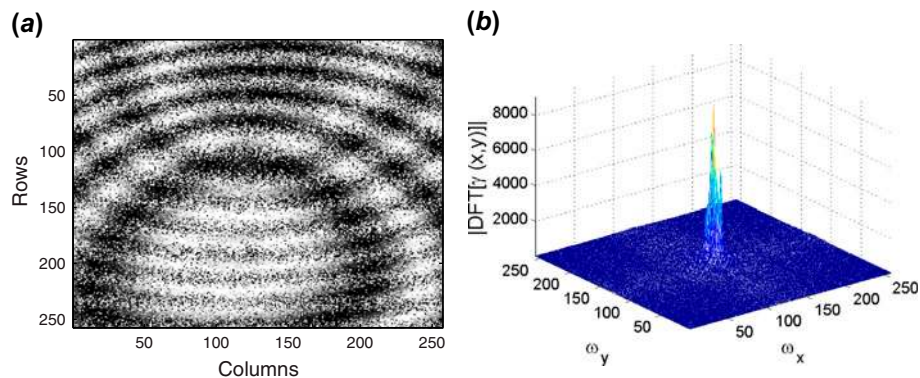

Figure 4. (*a*) Experimental moiré fringe pattern and (*b*) Fourier spectrum. (The color version of this figure is included in the online version of the journal.)

3. Simulation and experimental results

To evaluate the performance of the proposed method, the interference field in Equation (1) was simulated using two 2D interference phases, with the signal-to-noise ratio (SNR) of 30 dB. The size of simulated interference field was 513×513 pixels. The amplitude discrimination criteria with $A_1 = 2$ and $A_2 = 1$ were used. The moiré fringe pattern i.e. the real part of the interference field is shown in the Figure 1(*a*). The Fourier spectrum of the interference field shown in the Figure 1(*b*), indicates that the individual signal
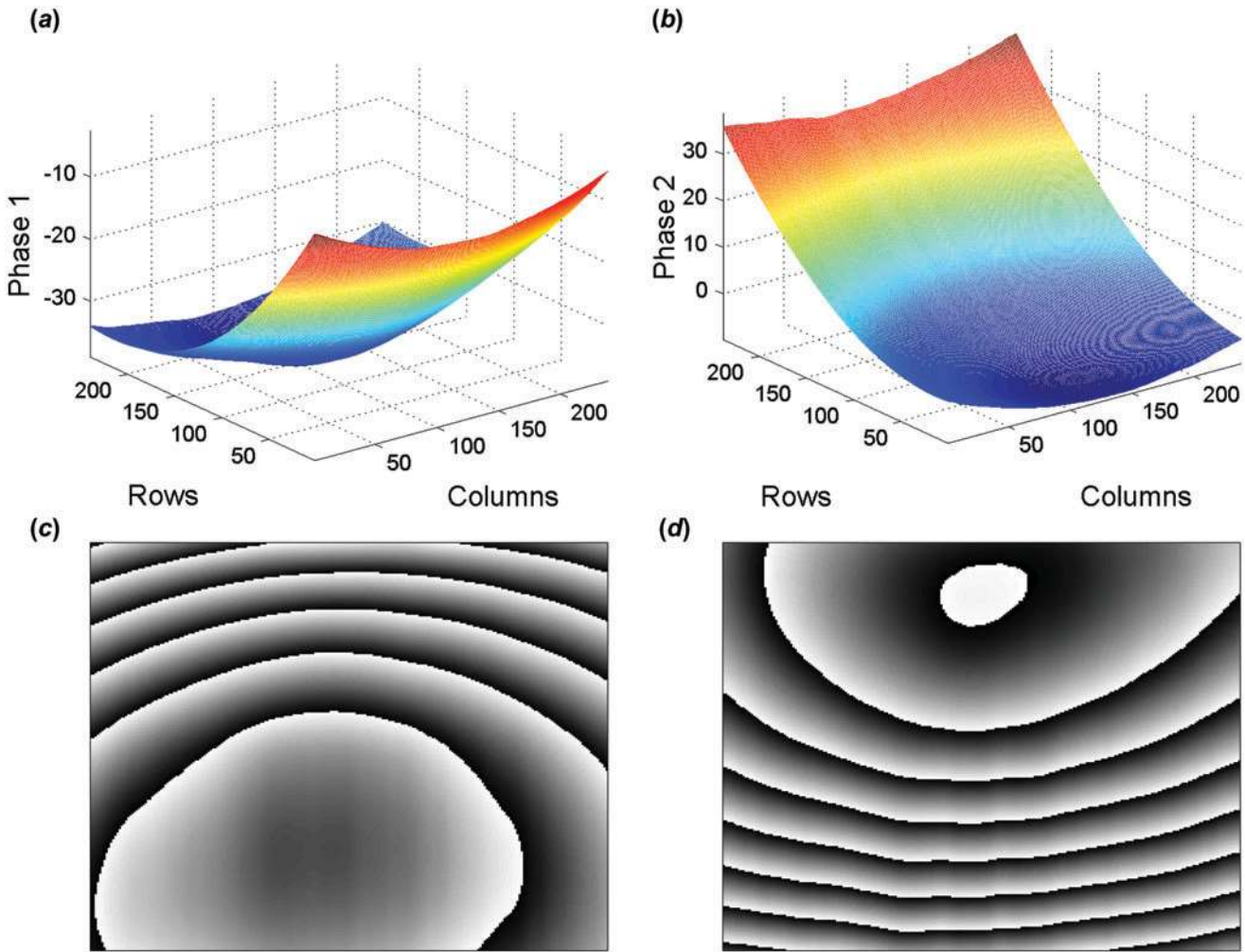
Figure 5. (*a*) Phase ϕ_1, (*b*) Phase ϕ_2, (*c*) wrapped form of ϕ_1 and (*d*) wrapped form of ϕ_2. (The color version of this figure is included in the online version of the journal.)

components are not well separated in the frequency domain. Therefore, the phase estimation methods based on spectral analysis [1] are not suitable for the analysis of the type of multicomponent signals we are concerned with.

The simulated interference phases ϕ_1 and ϕ_2 are shown in Figure 2(*a*) and (*b*), respectively. The interference field was divided into $N_w = 4$, number of segments in each column. The proposed method was applied for interference phase and phase derivative estimation. The error in the phase estimation is shown in Figure 2(*c*) and (*d*). The root mean-square-error (RMSE) in phase estimation was found to be 0.0286 and 0.0382 rad. The simulated interference phase derivatives of ϕ_1 and ϕ_2 are shown in Figure 3(*a*) and (*b*), respectively. The error in the phase derivative estimation is shown in Figure 3(*c*) and (*d*). The RMSE in phase derivative estimation was found to be 0.0078 and 0.0091 rad. The analysis was also performed with the method proposed in [17]. In that case, however, the RMSE in phase estimation was found to be 0.3386 and 0.3663 rad. As one can

see, these values are much higher as compared to those obtained by the method proposed in this paper. Moreover, the method proposed in [17] failed to produce faithfully the phase derivative estimation.

A digital holographic moiré configuration in which the object surface is illuminated by two collimated beams placed symmetrically with respect to the surface normal was set up to obtain moiré fringes. Since the proposed method does not require the spectra of the individual signal components to be separated, no carrier frequency needs to be introduced in the object beam. This overcomes the limitation of careful control of carrier frequency as required in [15]. To establish the amplitude discrimination criteria, the intensities of the two object beams were adjusted such that the intensity of one beam is twice as that of the other beam.

In the experimental setup, a Coherent Verdi (Coherent Inc., USA) laser of 532 nm wavelength was used as the light source. A CCD camera (XCL-U1000, Sony Corporation, Japan) of size 1600×1200 pixels was used for the recording
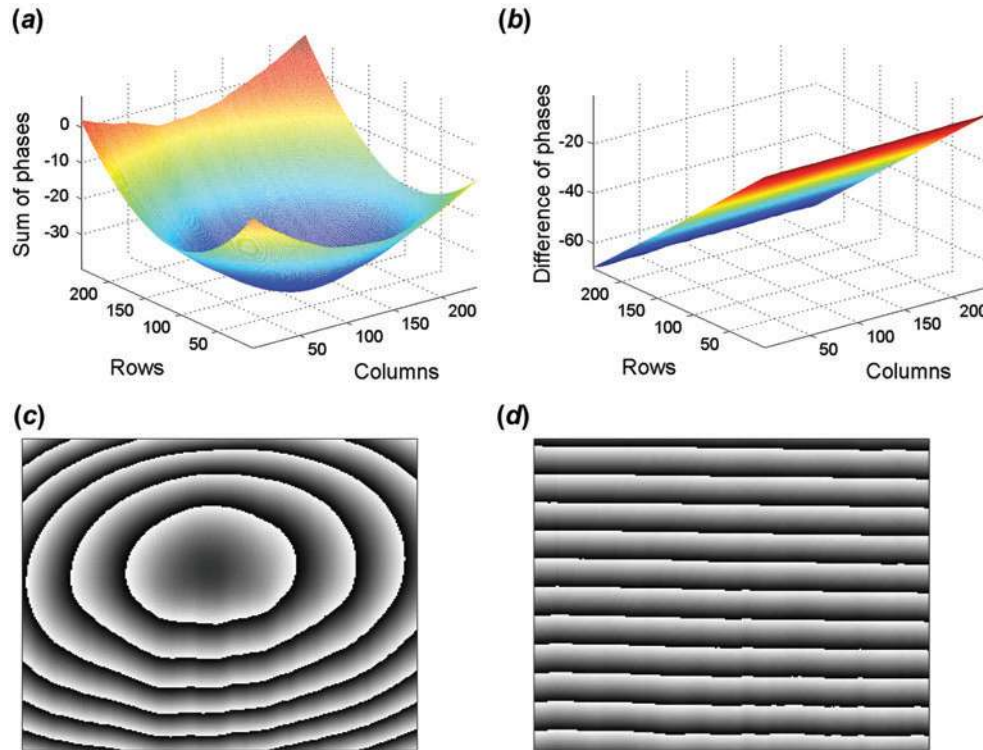
Figure 6. (*a*) Sum of phases, (*b*) Difference of phases, (*c*) wrapped form of sum of phases and (*d*) wrapped form of difference of phases. (The color version of this figure is included in the online version of the journal.)
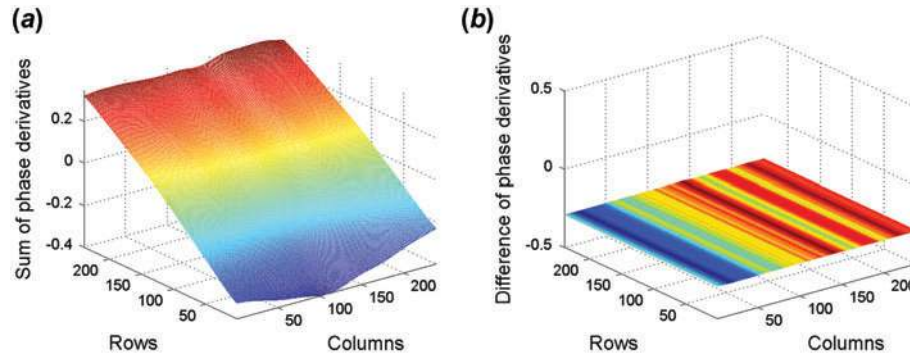

Figure 7. (*a*) Sum of phase derivatives and (*b*) Difference of phase derivatives. (The color version of this figure is included in the online version of the journal.)

of holograms. The real part of the reconstructed interference field, i.e. the digital holographic moiré fringe pattern is shown in Figure 4(*a*). The 2D Fourier transform of the interference field is shown in Figure 4(*b*). The unwrapped interference phases encoded in the moiré pattern were extracted using the proposed method as shown in Figure 5(*a*) and (*b*). The wrapped forms of the phases are shown in Figure 5(*c*) and (*d*). The sum and difference of estimated interference phases are shown in Figure 6(*a*) and (*b*) along with their wrapped forms in Figure 6(*c*) and (*d*), respectively. The phase derivative estimates were also calculated using the proposed method. The sum and difference of estimated

interference phase derivatives are shown in Figure 7(*a*) and (*b*).

4. Conclusion

A new approach for simultaneous measurement of multidimensional deformation is presented. The method reliably estimates the multiple interference phases and phase derivatives from a single digital holographic moiré fringe pattern without using any unwrapping algorithms or numerical differentiation. This makes the proposed method suitable for dynamic multidimensional deformation measurement. The

simulation results show that the proposed method performs better in term of accuracy as compared to the previously reported methods. The optical setup is simplified with the use of a single reference beam and a single laser source. The simulation and experimental results substantiate the effectiveness of the proposed method.

References

[1] Takeda, M.; Ina, H.; Kobayashi, S. *J. Opt. Soc. Am.* **1982,** *72,* 156–160.

[2] Kemao, Q. *Opt. Laser. Eng.* **2007,** *45,* 304–317.

[3] Watkins, L.R. *Opt. Laser. Eng.* **2012,** *50,* 1015–1022.

[4] Servin, M.; Marroquin, J.L.; Cuevas, F.J. *Appl. Opt.* **1997,** *36,* 4540–4548.

[5] Gorthi, S.S.; Rastogi, P. *J. Opt. A: Pure Appl. Opt.* **2009,** *11* (6), 1–6.

[6] Gorthi, S.S. *Rev. Sci. Instrum.* **2009,** *80* (7), 073109-1–073109-5.

[7] Hossain, M.M.; Sheoran, G.; Kumar, V.; Shakher, C. *Appl. Opt.* **2012,** *51,* 5331–5339.

[8] Wagner, C.; Seebacher, S.; Osten, W.; Jüptner, W. *Appl. Opt.* **1999,** *38,* 4812–4820.

[9] Baumbach, T.; Osten, W.; Von Kopylow, C.; Jüptner, W. *Appl. Opt.* **2006,** *45,* 925–934.

[10] Picart, P.; Moisson, E.; Mounier, D. *Appl. Opt.* **2003,** *42,* 1947–1957.

[11] Pedrini, G.; Tiziani, H.J. *Opt. Laser Tech.* **1997,** *29,* 249–256.

[12] Saucedo-A, T.; De La Torre-Ibarra, M.H.; Mendoza Santoyo, F.; Moreno, I. *Opt. Express* **2010,** *18,* 19867–19875.

[13] Picart, P.; Mounier, D.; Desse, J.M. *Opt. Lett.* **2008,** *33,* 276–278.

[14] Okazawa, S.; Fujigaki, M.; Morimoto, Y.; Matui, T. *Appl. Mech. Mater.* **2005,** *3–4,* 223–228.

[15] Rajshekhar, G.; SivaGorthi, S.; Rastogi, P. *Appl. Opt.* **2011,** *50,* 4189–4197.

[16] Rajshekhar, G.; Gorthi, S.S.; Rastogi, P. *Opt. Express* **2012,** *20,* 1281–1291.

[17] Kulkarni, R.; Rastogi, P. *Opt. Lasers Eng.* **2013,** *51,* 1168–1172.

[18] Wang, P.; Djurovic, I.; Yang, J. *Chinese J. Elec.* **2008,** *17,* 189–194.

[19] Wang, P.; Yang, J. *Digit. Signal Process. Rev. J.* **2006,** *16,* 654–669.

[20] Aboutanios, E.; Mulgrew, B. *IEEE Trans. Signal Process.* **2005,** *53,* 1237–1242.

[21] Pham, D.S.; Zoubir, A.M. *IEEE Trans. Signal Process.* **2007,** *55,* 56–65.